Catalysis Today 142 (2009) 24–29

Contents lists available at ScienceDirect

Catalysis Today

journal homepage: www.elsevier.com/locate/cattod

Oxidation of methane on nanoparticulate Au/TiO_2 at low temperature: A combined microreactor and DFT study

G. Walther [a], G. Jones [a], S. Jensen [b], U.J. Quaade [c], S. Horch [a,*]

[a] Center for Atomic-scale Materials Design (CAMD), Department of Physics, Technical University of Denmark, DK-2800 Kgs. Lyngby, Denmark
[b] Department of Micro and Nanotechnology (MIC), Technical University of Denmark, DK-2800 Kgs. Lyngby, Denmark
[c] Center for Individual Nanoparticle Functionality (CINF), Department of Physics, Technical University of Denmark, DK-2800 Kgs. Lyngby, Denmark

ARTICLE INFO

Article history:
Available online 23 February 2009

Keywords:
Gold
Titanium dioxide
Catalysis
Microreactor
Methane
Oxidation
Particle size

ABSTRACT

Herein we present results from experimental and theoretical studies concerning low temperature oxidation of CH_4 over TiO_2 supported Au nanoparticles. Our findings suggest that partial oxidation cannot be achieved under these conditions (1 bar, 30–250 °C). In order to understand this further, results from CO and H_2 oxidation studies are also presented. The reaction rate for CH_4 oxidation is found to be far lower than the rate for both CO and H_2 oxidation, this goes towards explaining the strong tendency for total CH_4 oxidation. These findings are further corroborated by DFT-calculations investigating the thermodynamics of CH_4 oxidation on a stepped Au(2 1 1) surface.

1. Introduction

There is continued interest to find catalysts which can transform CH_4 into an easily transportable liquid via low-temperature partial oxidation of CH_4. This is mainly due to the fact that large amounts of natural gas are available in areas that are so remote from the energy consumers that there are no pipelines available to transport the gas. Presently, direct liquefaction of CH_4, the main component of natural gas, is the most common process used for shipping in gas tankers. This requires low temperatures and high pressure and is thus not really an economically viable option. Instead, more than 20 billion cubic meters of natural gas are flared annually which has a detrimental effect on the environment [1]. Unfortunately however, no good catalyst is known so far for low-temperature partial CH_4 oxidation. The reason is that methanol dissociates catalytically at lower temperatures than partial methane oxidation occurs. The search is on therefore, to find a catalyst that provides the required selectivity.

The quest for partial oxidation catalysts is also important for the increasing market in CH_4, which represents one of the basic organic chemicals [2]. In this connection, much work is being carried out in order to develop new catalysts that can convert CH_4 into higher-value chemicals [3,4]. Baiker and co-workers have studied a number of noble metals catalysts to determine their potential for the partial oxidation of CH_4 to CO and H_2. They have recently reported identification of extinction and ignition temperature rates and selectivity between 300 °C and 500 °C [5]. In an earlier study, Iglesia and Wei studied the reaction of different gas mixtures containing CH_4, CO_2 and labeled CO over supported platinum clusters [6]. Since identical ^{13}C fractions in CO and CO_2 were determined, Iglesia and Wei concluded that CO_2 activation is quasi-equilibrated and kinetically irrelevant. Recent studies suggest that there is a condition dependent mechanism for the reforming reaction of CH_4 with CO formation being dominant at lower temperatures and CH_4 activation taking over at higher temperature [7]. However it must be kept in mind that these experiments and calculations are looking at the CH_4 reforming reaction, which is run at temperatures in the range of 600–800 °C.

Within the last decade, a new candidate for such a catalyst, nanoparticulate gold, has emerged. Even though gold is often referred to as the noblest of all the metals (it is, e.g. inert in an oxygen atmosphere [8]), nanoparticulate gold shows a surprisingly high catalytic activity for CO oxidation in both experimental [9–20] and theoretical studies [19,21–27]. Beside CO oxidation, many other reactions have been studied on gold catalysts, including the oxidation of hydrocarbons [18,19,28–31] and oxygen-containing hydrocarbons [11,18,19,32,33] as well as the catalysis of hydrogenation of unsaturated substrates [11,19,34].

* Corresponding author.
E-mail address: horch@fysik.dtu.dk (S. Horch).

0920-5861/$ – see front matter © 2009 Elsevier B.V. All rights reserved.
doi:10.1016/j.cattod.2009.01.007

The reason for this surprising activity is still under debate: After the pioneering work of Haruta [9], the activity of gold has been linked to several different effects, e.g. a quantum-size effect [10], support-induced strain [22], charge transfer from the small gold particles to adsorbed oxygen [35] and the role of low-coordinated gold atoms [22,24–27]. It is clear from these alternative perspectives that more work is required to find the definitive answer to this debate. However it is entirely probable that any of the perspectives are correct under a given set of reaction conditions, and that the apparent results are sometimes the results of experimental or theoretical conditions and probe being used.

Another issue when using gold as a catalyst is the stability of nanoparticulate gold. Since gold has a low melting point, gold nanoparticles become mobile even at low temperatures [36–38], and are observed to sinter into bigger particles [37]. An effective support which is able to keep the gold particles well dispersed (and the one we also use in this contribution) is TiO_2. However, more study is needed to figure out how this works, and to understand fully how the particles change during reaction.

In the present contribution, we present a combined experimental and theoretical study of low-temperature CH_4 oxidation on nanoparticulate gold supported on TiO_2. We focus particularly on the possible reasons why partial oxidation cannot be achieved. To this end, we compare the experimental findings with a thermodynamic picture for CH_4 oxidation, obtained from density functional theory (DFT) calculations. Additionally, the influence of the reaction to the gold particles was investigated.

2. Experimental section

2.1. Experimental setup

Activity measurements of supported gold nanoparticles were performed in microreactors. The capillaries of these silicon devices were etched using deep reactive ion etching (DRIE). The fabrication process is described elsewhere [39,40]. Fig. 1a illustrates the 280 μm deep capillary system consisting of two inlets, a sniffer hole and one outlet. It allows mixing of undiluted gases on the chip without any danger of explosion. The dimensions of the reactor chamber are $(8.0 \times 1.5 \times 0.2)\text{mm}^3$. The whole device measures 20 mm × 16 mm × 0.35 mm and is closed with a Pyrex glass lid using anodic bonding. The inlet and outlet holes as well as the sniffer hole are sealed with Viton O-rings to an aluminum interface block. The reactor chamber can be heated by a piece of silicon that is clamped to it. Temperature is measured with a K-type thermocouple on the top of the reactor. For temperature-ramped activity measurements, temperature is controlled using a PID-controller (Eurotherm). Gas flow is controlled by mass flow controllers (Bronkhorst), operating in the range from 0.02 to 1.00 ml min^{-1} with a precision of 0.02 ml min^{-1}. Via the sniffer hole, the microreactor is connected to a Baltzers quadrupole mass spectrometer (QMA) to analyze the reaction products. Fig. 1b and c show a zoom-in on the 3 μm sniffer hole.

To confirm the QMA analysis, an Agilent gas chromatograph (3000A microGC) was used to analyze the reaction products. Since the GC is less sensitive than the QMA, a mini-reactor (quartz glass tube) containing more catalyst material was used in that case to produce larger amounts of the reaction products. The GC has combined columns of 10 m molecular sieve and 3 m PLOT U with 1.0 μl back-flushing, which allows simultaneous analysis of H_2, O_2, N_2, CO, CO_2, H_2O and CH_4 by a thermal conductivity detector (TCD). With argon as the carrier gas, the GC is 15 times more sensitive to H_2 than to CO. To avoid condensing water, formed by the catalytic reactions, the tubing between the microreactor and the GC is kept at a temperature of 100 °C, whereas the capillary of the GC itself is kept at 90 °C.

2.2. Catalytic reactions

A 3.3 nm Au/TiO_2 reference catalyst from the World Gold Council was used to study total CH_4 oxidation according to formula (1). We also considered partial CH_4 oxidation (2) and studied therefore the oxidation of CO (3) and H_2 (4) as well, using a fresh catalyst for each reaction.

$$CH_4 + 2O_2 \rightarrow CO_2 + 2H_2O, \quad \Delta H^0 = -802.3\,\text{kJ mol}^{-1}, \tag{1}$$

$$CH_4 + \tfrac{1}{2}O_2 \rightarrow CO + 2H_2, \quad \Delta H^0 = -185.3\,\text{kJ mol}^{-1}, \tag{2}$$

$$CO + \tfrac{1}{2}O_2 \rightarrow CO_2, \quad \Delta H^0 = -283.0\,\text{kJ mol}^{-1}, \tag{3}$$

$$H_2 + \tfrac{1}{2}O_2 \rightarrow H_2O, \quad \Delta H^0 = -241.8\,\text{kJ mol}^{-1}. \tag{4}$$

Due to the high sensitivity of the GC to hydrogen, the reactants in (4) were diluted with 50% argon. For all reactions discussed, the total flow was kept constant at 1.00 ml min^{-1}.

Self heating of the catalyst during an exothermic reaction is difficult to avoid, but it can be minimized by operating the catalyst in a range up till 10% conversion. The greatest amount of heat liberated during the above reactions was 26.0 mW for CO oxidation, where 40% conversion was already achieved at 80 °C.

The catalysts used both in the microreactor as well as in the mini-reactor were deactivated over 18 h at 100 °C. To ensure reproducibility, activity measurements were conducted afterwards with the following scheme for the applied CH_4/O_2 ratio, which was run twice: 2/1, 4/1, 1/2. Reproducibility of the first and the second GC-run was taken as sign for that the catalyst did not change during reactions. For steady-state activity measurements, the temperature was ramped from 50 °C to 250 °C in steps of 10 °C h^{-1} when using the GC and from 75 °C to 225 °C in steps of 5 °C per 5 min when using the QMA.

2.3. Particle analysis

The size distribution and shape of the gold particles were probed using a PHILIPS Tecnai 20T high resolution transmission electron microscope at 200 kV. Specimens of the catalyst were

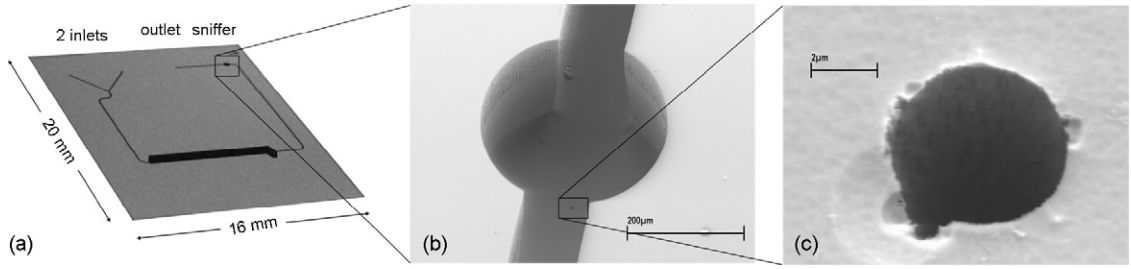

Fig. 1. Unloaded silicon microreactor with two inlets to mix gases on the chip, a $(8.0 \times 1.5 \times 0.2)\text{mm}^3$ sized reactor chamber, a sniffer hole and a single outlet.

taken before and after the temperature-programmed activity measurements, and prepared on a carbon TEM grid by dropping a suspension of catalyst in ethanol on the grid.

2.4. Theoretical methodology

DFT is used as implemented in the computer code DACAPO using the RPBE exchange correlation functional [41]. Calculations for stepped model gold surfaces were carried out using fcc crystals terminated at the {2 1 1} facet. Unit cells of (2×1) periodicity were used with a depth of 10 atomic layers (roughly equivalent to 3-close packed layers) and a vacuum region of 10 Å. An electronic planewave cut-off of 340 eV has been used with the Brillouin zone being sampled by a Monkhorst-Pack [42] mesh of $4 \times 4 \times 1$ k-points. Pseudopotentials of the Vanderbilt [43] type were used to describe the electronic core regions.

Thermodynamic analysis is carried out using the total energies obtained from the DFT-calculations. In this paper free energies have been calculated by employing standard formulas for the thermodynamics of a classical ideal gas [44]. For a gas-phase species (X) at temperature (T) and pressure (P), the Gibbs free energy ($G_X^{P,T}$) is given by:

$$G_X^{P,T} = E_X + E_{ZPE} + \Delta H^{0,T} - TS^T + RT\ln(P/P^o),$$

where E_{ZPE} is the zero point energy, $\Delta H^{0,T}$ is the enthalpy change due to raising the temperature from 0 K to T, S^T is the entropy at T, R is the universal gas constant and P^o is standard pressure (taken to be 1 bar).

The potential energy of the adsorbed species (X'), $E_{X'}$, is given by: $E_{Au/X'} - E_{Au,}$ where E_{Au} is the energy of the clean Au surface and $E_{Au/X'}$ is the energy of the adsorbate and surface system. In order to calculate the free energy of this species we neglect the pressure term so that the enthalpy change is replaced by the change in internal energy. This leads to the following expression for the free energy ($G_{X'}^{P,T}$):

$$G_{X'}^{P,T} = E_{X'} + E_{ZPE} + \Delta U^{0,T} - TS^T.$$

All vibrational frequencies used to determine E_{ZPE}, $\Delta U^{0,T}$ and S^T are calculated within the harmonic approximation.

It is an unfortunate deficiency on the current implementations of DFT that the exchange correlation functional does not handle self-interaction correctly. This is particularly troublesome for calculations involving the gas-phase O_2 molecule and adsorbed CO. In order to overcome these deficiencies of DFT it is possible to apply empirical corrections. This paper has implemented the correction proposed by Abild-Pedersen and Andersson for CO adsorption [45]. In order to correct for the O_2 molecule we make a correction that essentially involves comparing the calculated Gibbs energy of formation for water with that obtained experimentally. Any discrepancy between the two values is attributed to the O_2 molecule, details of the correction implemented herein can be found in Appendix 1.

3. Results

The average gold particle size before activity measurements was determined to be (3.4 ± 0.8) nm based on a TEM-analysis of 60 particles, as illustrated in Fig. 2. This equals the value stated by the supplier, indicating that the particles had not sintered during storage.

3.1. Methane oxidation

The apparent activation energy for CH_4 oxidation on these particles was determined to be approximately (60 ± 2) kJ mol^{-1} from the Arrhenius plots in Fig. 3. The difference in reaction rate when measured with the QMA or the GC may be related to a morphological change of the catalyst in the GC-runs, since the time the catalyst was exposed to the reactants was 24 h for each GC measurement as compared to only 3 h in case of the QMA. This accounts also for the higher conversion, plotted in Fig. 4, when the measurement was conducted using a QMA. Since neither CO nor H_2 were detected, the yield of CO_2 is directly given by the consumption of CH_4. The onset of CH_4 oxidation was found at 130 °C.

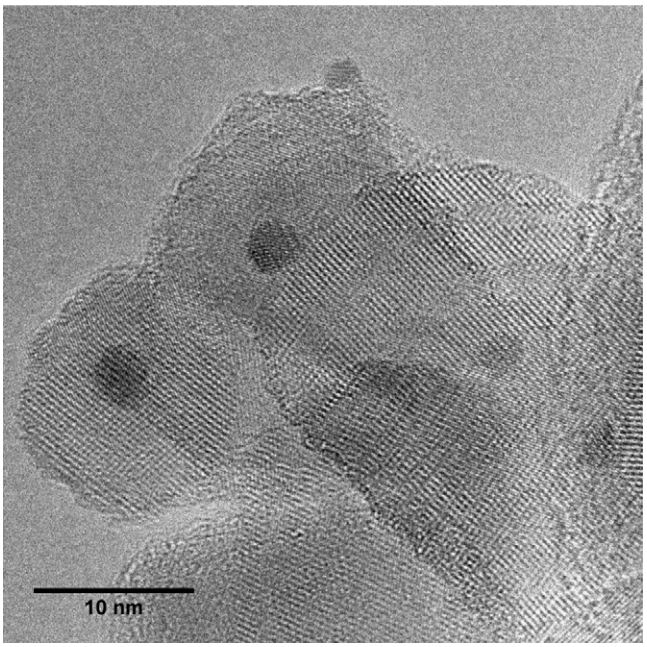

Fig. 2. High resolution TEM image of the catalyst as supplied.

TEM-analysis after the entire sequence of steady-state CH_4 oxidation measurements in the GC shows that the particles now have a broad range of sizes (2–7 nm). By tilting the specimen from −65° to +65°, the three dimensional structure of the particles can be reconstructed. We did this for one particle: Fig. 5 shows a TEM image of a 4.8 nm gold particle with its 3D reconstruction (see inset). This particle is found to stick to the support with its (1 1 1) surface, as indicated by the arrow.

3.2. CO and H_2 oxidation

The parallel running fits for CO and H_2 oxidation in the Arrhenius plot (Fig. 6) indicate similar activation energies for both

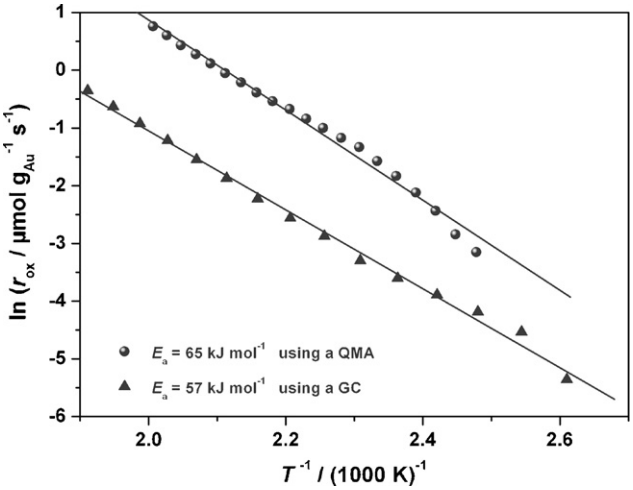

Fig. 3. Arrhenius plots of the CH_4 oxidation rates. The uncertainty of E_a is ~2 kJ mol^{-1} and 1 kJ mol^{-1} when using the QMA and the GC setup, respectively.

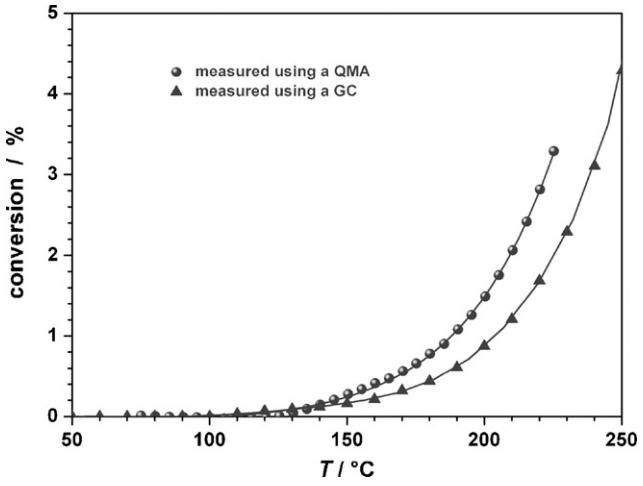

Fig. 4. CH_4 conversion shows an onset at 130 °C.

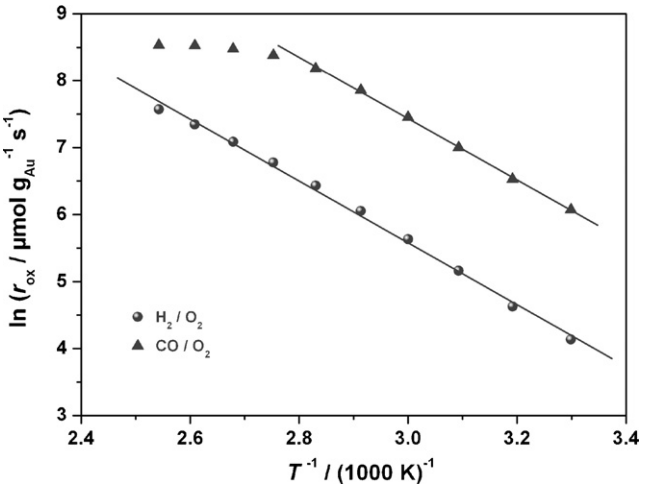

Fig. 6. Arrhenius plots of the CO and H_2 oxidation rates determined using the GC.

reactions. From the Arrhenius equation, the activation energy could be determined to be (38 ± 0.8) kJ mol^{-1} for CO oxidation. The reaction rate for H_2 oxidation is about 6 times lower than that for CO oxidation. This goes along with the higher conversion of CO than H_2 as function of temperature, represented in Fig. 7. For CO oxidation, saturation was already found at 80 °C. For both reactions, a mass balance of the reactants consumed and the products formed was used to verify the results.

The particle size of the freshly prepared gold after these sequences of steady-state CO- or H_2-oxidation measurements in the GC was determined to be (5.7 ± 3.4) nm by TEM-analysis of 57 particles.

3.3. Theoretical results

Fig. 8 illustrates the standard free energy diagram for the stable species present in the oxidation of CH_4 at 450 K. This is constructed using the DFT total energies in combination with the thermodynamic corrections as outlined in the methodology. Three possible pathways are depicted, partial oxidation terminating at CO(g) and H_2(g), also CO_2(g) and H_2(g) and finally complete combustion to CO_2(g) and H_2O(g). The diagram shows a route which goes via a

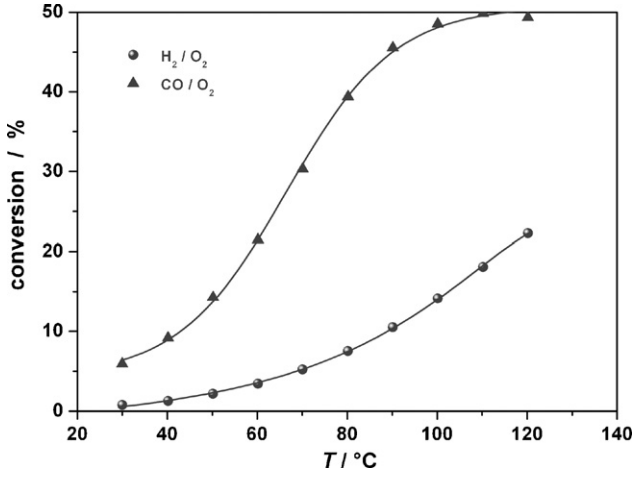

Fig. 7. Conversion of CO and H_2.

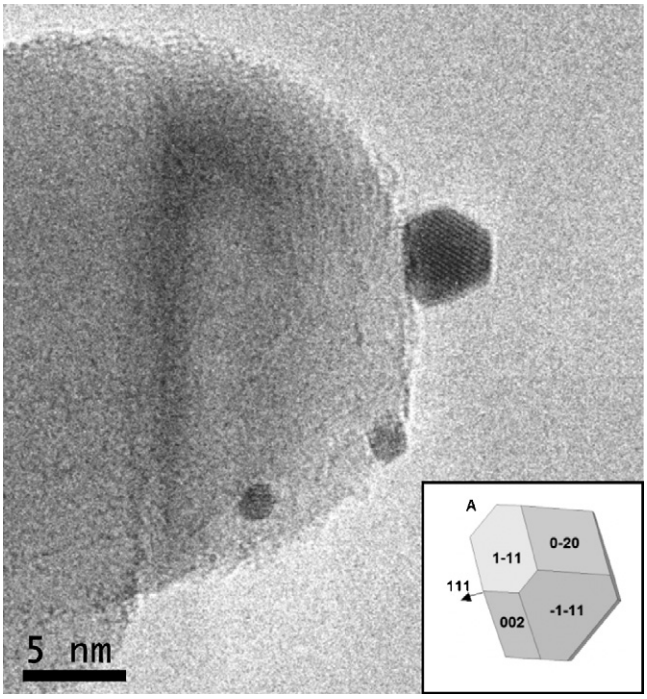

Fig. 5. High resolution TEM image of a 4.8 nm gold particle after steady-state activity measurements.

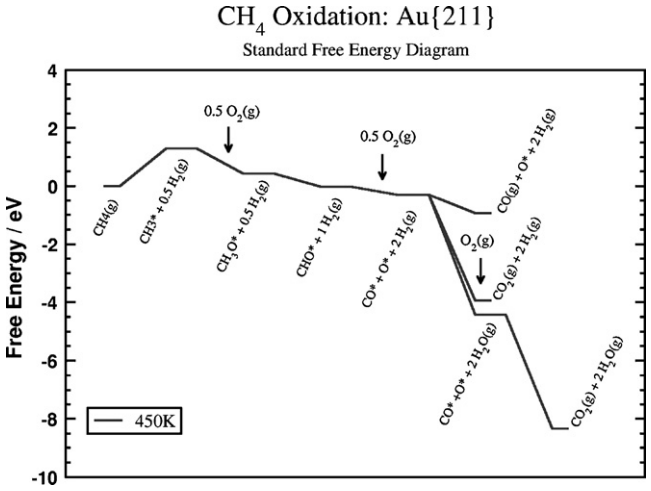

Fig. 8. Standard free energy reaction profile for the stable intermediates present in the oxidation of CH_4, as determined from DFT.

methoxy intermediate followed by carbonyl species on the surface prior to the formation of CO(g) (CO_2(g)). It was found that if one went via a route of direct dehydrogenation of CH_4 then the thermodynamic barriers were extremely high (in excess of 4 eV for the formation of C* + 2H_2(g) from CH_4). It can be seen that this route still contains the difficult initial dehydrogenation of CH_4, which is 1.4 eV uphill. However once this step is overcome the pathway is downhill all the way to the products. Here we see that complete combustion is by far the most thermodynamically favored reaction and consequently (subject to kinetic barriers) one would expect the reaction to proceed to this point. Indeed this is found to be the case experimentally where partial oxidation is not observed, we will revisit this point in Section 4.

4. Discussion

We shall start by considering the species present, as detected during the experimental run. In the case of partial oxidation, we can assume (due to the stoichiometry of the reaction) that if we were to form CO during CH_4 oxidation, then H_2 would also be formed (2). In fact, we did not observe any H_2 evolution, our first indication of the lack of partial oxidation. Furthermore we did observe water formation during the CH_4 oxidation, in proportions that match the stoichiometry expected from Eq. (1). From this we can conclude that we have carried out complete combustion to form CO_2.

The results of additional studies on the oxidation of H_2 and CO, their activation barriers, rates and conversions are shown in Table 1. These suggest that even if CO was formed from partial oxidation, CO and H_2 could easily be post-oxidized to CO_2 and H_2O. This is due to the fact that when compared to CH_4 oxidation, the higher reaction rate for CO and H_2 oxidation (which is coupled to their lower apparent activation energies (38 ± 0.6) kJ mol^{-1}), indicates that under these reaction conditions these steps would be equilibrated.

We have carried out the theoretical calculations on a {2 1 1} surface, and shall first address some of the issues surrounding this as a model system. This particular surface facet has been chosen because recent experimental and theoretical work has demonstrated the importance of the B5 site in catalytic activity for N_2 dissociation and CH_4 activation on Ni [46]. If one looks at the {2 1 1} surface, it can be seen that the step sites are made up of the B5 sites. Therefore we expect this surface to be a good model of the edges and steps present on a nanoparticle. Some care does however need to be taken because corner sites may also be implicated in the activity of a catalyst, this in fact is the subject of on going research. However, in our case we anticipate the model to be reasonable in the explanation of reactivity.

If we look at the thermodynamic picture presented from theory we are able to gain insight into whether a particular reaction is feasible. In fact what we see from Fig. 8 is that both partial CH_4 oxidation and complete CH_4 combustion are exothermic at 450 K, meaning both processes are likely to proceed. However, CO_2(g) formation is favored far more greatly and in the absence of kinetic considerations would dominate the oxidation process. Experimentally we never observe evidence for the formation of CO(g) or H_2(g) above that of the background noise which concurs well with this simple analysis.

Table 1
Comparison of activation energies, reaction rates and conversion.

Reaction	E_a/kJ mol^{-1}	ln(r_{ox}/μmol g_{Au}^{-1} s^{-1})	Conversion/%
CH_4/O_2	61 ± 4	0.7 (at 220 °C)	2.9 (at 220 °C)
CO/O_2	38 ± 0.6	8.3 (at 80 °C)	45 (at 80 °C)
H_2/O_2	38 ± 0.8	6.4 (at 80 °C)	7 (at 80 °C)

In order to go beyond just the thermodynamic picture, one needs to consider the barriers present in the reaction pathway. Recent work by Nørskov and co-workers has studied the oxidation of CO on a model nanoparticle [27]. Their work demonstrated that there are two possible routes by which complete oxidation can proceed. The first is by reaction with adsorbed atomic oxygen O* (* denotes an adsorbed species). The second is through an intermediate that involves molecular oxygen, this is generally perceived to proceed via a physisorbed precursor. This particular mechanism has also been highlighted by Alavi and co-workers [23]. Both of these works showed good agreement on the relative barrier heights to CO oxidation, with the barrier via the first route being approximately 63 kJ mol^{-1} and that of the second route being 39 kJ mol^{-1}. This is in good agreement with our apparent activation barrier of CO oxidation measured.

5. Conclusions

In the present paper, we have investigated CH_4 oxidation on TiO_2 supported gold nanoparticles under mild conditions (1 bar, 30–250 °C). Our experiments show that only total oxidation of CH_4 occurs. Additional studies of CO and H_2 oxidation strongly suggest that these species can easily be post-oxidized, even if partial CH_4 oxidation has occurred early in the reaction. From DFT-calculations, the thermodynamics show that there is a strong tendency for the formation of CO_2, which means the only way to achieve partial oxidation, is to exploit the variations in barrier heights, i.e. we are attempting to form the kinetic product – not a thermodynamic product. On a stepped Au(2 1 1) surface, CH_4 dissociation is shown to be thermodynamically unfavorable and the influence of barriers and kinetics on this process are the subject of ongoing work.

Acknowledgements

G. Walther gratefully acknowledges financial support from NABIIT. We thank Lionel Cervera Gontard (Center for Electron Nanoscopy, CEN.DTU) for experimental assistance with taking and analyzing TEM images. The Center for Atomic-scale Materials Design is funded by the Lundbeck Foundation. The authors wish to acknowledge additional support from the Danish Center for Scientific Computing through grant HDW-1103-06.

Appendix A

A.1. Correction to O_2(g)

This basis of this correction lies in taking an experimentally determined value for the formation of water which is obtainable from standard thermodynamic tables. This is then compared to the value obtained using DFT in combination with thermodynamic calculations, the difference between these two values is used to establish the correction required for the O_2 molecule (δ_{O_2}):

$$\delta_{O_2} = 2(\Delta_f G^{o,298}_{\text{Tables}} - \Delta_f G^{o,298}_{\text{calc.}}).$$

The factor of 2 arises due to the definition of the heat of formation of water being for the formation of one mole of water, from one mole of H_2 gas and half a mole of oxygen gas. We can thus define the standard Gibbs free energy of Reaction as:

$$\Delta_f G^{o,298} = \Delta G^{o,298}_{H_2O} - \Delta G^{o,298}_{H_2} - \frac{1}{2}\Delta G^{o,298}_{O_2}$$

The expression for the Gibbs free energy of the individual species can be found in the theoretical methodology.

Table 2 lists the key values that are required to find the correction, determined both from DFT-calculations and by application of the

Table 2
Thermodynamic properties calculated from both the partition function and from tabulated values in parenthesis. Enegies/eV.

Species	E_{ZPE}	ΔH^{0-298}	TS^{298}	$\Delta_f G^{o,298}$
H_2O	0.58(0.56)	0.10(0.10)	0.58(0.58)	−469.63(−469.65)
H_2	0.27(0.27)	0.09(0.09)	0.40(0.40)	−32.07(−32.07)
O_2	0.10(0.10)	0.09(0.09)	0.60(0.63)	−871.13(−871.16)
$H_2O–H_2–1/2O_2$	0.26(0.24)	−0.03(−0.03)	0.12(0.14)	−2.00(−2.00)

thermodynamics of a classical ideal gas. In parenthesis the values determined from thermodynamic tables are listed, as can be seen there is very little to separate these values from those obtained by theory. The CRC handbook lists the Gibbs free energy of formation at 298 K of water, $\Delta_f G^{o,298}(H_2O)$, as being −228.582 kJ mol^{-1} (−2.37 eV). The potential energy of formation, $\Delta_f E_{DFT}(H_2O)$, is found to be −2.35 eV, which combined with the thermodynamic values leads to a correction of 0.74 eV.

References

[1] V.S. Arutyunov, V.M. Rudakov, V.I. Savchenko, E.V. Sheverdenkin, O.G. Sheverdenkin, A.Yu. Zheltyakov, Theo. Found. Chem. Eng. 36 (2002) 472.
[2] N.D. Parkyns, C.I. Warburton, J.D. Wislon, Catal. Today 18 (1993) 385.
[3] C.-J. Liu, T. Hammer, R. Mallinson, Catal. Today 98 (VII) (2004).
[4] M.O. Adebajo, Green Chem. 9 (2007) 526.
[5] S. Hannemann, J.-D. Grunwaldt, P. Lienemann, D. Günther, F. Krumeich, S.E. Pratsinis, A. Baiker, Appl. Catal. A 316 (2007) 226.
[6] J. Wei, E. Iglesia, J. Phys. Chem. B 108 (2004) 4094.
[7] M.P. Andersson, F. Abild-Pedersen, I.N. Remediakis, T. Bligaard, G. Jones, J. Engbæk, O. Lytken, S. Horch, J.H. Nielsen, J. Sehested, J.R. Rostrup-Nielsen, J.K. Nørskov, I. Chorkendorff, J. Catal. 255 (2008) 6.
[8] J. Kim, E. Samano, B. Koel, Surf. Sci. 600 (2006) 4622.
[9] M. Haruta, Catal. Today 36 (1997) 153.
[10] M. Valden, X. Lai, D.W. Goodman, Science 281 (1998) 1647.
[11] G.C. Bond, Catal. Rev. Sci. Eng. 41 (1999) 319.
[12] M. Haruta, Catal. Technol. 6 (2002) 102.
[13] A.C. Gluhoi, M.A.P. Dekkers, B.E. Nieuwenhuys, J. Catal. 219 (2003) 197.
[14] B. Schuhmacher, V. Plzak, M. Kinne, R.J. Behm, Catal. Lett. 89 (2003) 109.
[15] M. Chen, D.W. Goodman, Science 306 (2004) 252.
[16] T.V.W. Janssens, A. Carlsson, A. Puig-Molina, B.S. Clausen, J. Catal. 240 (2006) 108.
[17] H.-J. Freund, Catal. Today 117 (2006) 6.
[18] D.T. Thompson, Top. Catal. 38 (2006) 231.
[19] G.C. Bond, C. Louis, D.T. Thompson, Catalysis by Gold, 1 Ed., Imperial College Press, London, 2006.
[20] C. Xu, J. Su, X. Xu, P. Liu, H. Zhao, F. Tian, Y. Ding, J. Am. Chem. Soc. 129 (2007) 42.
[21] B. Hammer, J.K. Nørskov, Surf. Sci. 343 (1995) 211.
[22] M. Mavrikakis, P. Stotze, J.K. Nørskov, Catal. Lett. 64 (2000) 101.
[23] Z. Liu, P. Hu, a. Alavi, J. Am. Chem. Soc. 124 (2002) 14770.
[24] N. Lopez, J.K. Nørskov, J. Am. Chem. Soc. 124 (2002) 11262.
[25] N. Lopez, T.V.W. Janssens, B.S. Clausen, Y. Xu, M. Mavrikakis, T. Bligaard, J.K. Nørskov, J. Catal. 223 (2004) 232.
[26] T.V.W. Janssens, B.S. Clausen, B. Hvolbæk, H. Falsig, C.H. Christensen, T. Bligaard, J.K. Nørskov, Top. Catal. 44 (2007) 15.
[27] B. Hvolbæk, T.V.W. Janssens, B.S. Clausen, H. Falsig, C.H. Christensen, J.K. Nørskov, NanoToday 2 (2007) 14.
[28] R.D. Waters, J.J. Weimer, J.E. Smith, Catal. Lett. 30 (1994) 181.
[29] S. Ivanova, C. Petit, V. Pitchon, Catal. Today 113 (2006) 182.
[30] S. Ivanova, C. Petit, V. Pitchon, Gold Bull. 39 (2006) 3.
[31] B.E. Solsona, T. Garcia, C. Jones, S.H. Taylor, A.F. Carley, G.J. Hutchings, Appl. Catal. A 312 (2006) 67.
[32] A.S.K. Hashmi, G.J. Hutchings, Angew. Chem. Int. 45 (2006) 7896.
[33] C.H. Christensen, B. Jørgensen, J. Rass-Hansen, K. Egeblad, R. Madsen, S.K. Klitgaard, S.M. Hansen, M.R. Hansen, H.C. Andersen, A. Riisager, Angew. Chem. Int. Ed. 45 (2006) 4648.
[34] M.-C. Daniel, D. Astruc, Chem. Rev. 104 (2004) 293.
[35] J.A.v. Bokhoven, C. Louis, J.T. Miller, M. Trommp, O.V. Safonova, P. Glatzel, Angew. Chem. 118 (2006) 4767.
[36] P. Buffat, J.P. Borel, Phys. Rev. A 13 (1976) 2287.
[37] E. Charls, H. Sykes, F.J. Williams, M.S. Tikhov, R.M. Lambert, J. Phys. Chem. B 106 (2002) 5390.
[38] P.M. Ajayan, D.L. Marks, Phys. Rev. Lett. 60 (1988) 585.
[39] U.J. Quaade, S. Jensen, O. Hansen, Rev. Sci. Instrum. 75 (2004) 3345.
[40] U.J. Quaade, S. Jensen, O. Hansen, J. Appl. Phys. 97 (2005) 044906.
[41] B. Hammer, L.B. Hansen, J.K. Nørskov, Phys. Rev. B 59 (1999) 7413.
[42] H.J. Monkhorst, J.D. Pack, Phys. Rev. B 13 (1976) 5188.
[43] D. Vanderbilt, Phys Rev. B 41 (1990) 7892.
[44] J.H. Noggle, Physical Chemistry, Little, Brown and Co., 1985.
[45] F. Abild-Pedersen, M.P. Andersson, Surf. Sci. 601 (2007) 1747.
[46] F. Abild-Pedersen, O. Lytken, J. Engbæk, G. Nielsen, I. Chorkendorff, J.K. Nørskov, Surf. Sci. 590 (2005) 127.